Solid Freeform Fabrication 2022: Proceedings of the 33rd Annual International Solid Freeform Fabrication Symposium – An Additive Manufacturing Conference
Reviewed Paper

Effect of thermal post-processing on microstructure and tensile behavior of additively manufactured aluminum alloys (AlSi10Mg and Scalmalloy) via L-PBF: A comparative study

Md Faysal Khan[1,2], Shaharyar Baig[1,2], Seyed R. Ghiaasiaan[1,2], Paul R. Gradl[3], Shuai Shao[1,2], Nima Shamsaei[1,2*]

[1]National Center for Additive Manufacturing Excellence (NCAME), Auburn University, Auburn, AL 36849, USA

[2]Department of Mechanical Engineering, Auburn University, Auburn, AL 36849, USA

[3]Propulsion Department, NASA Marshall Space Flight Center, Huntsville, Al 35812, USA

* Corresponding author:

Email: shamsaei@auburn.edu

Tel: (334) 844 4839

Abstract

Additively manufactured aluminum (Al) alloys have recently received growing interest from different industrial sectors. This study compares the microstructure and tensile properties of two laser powder bed fused Al alloys, namely AlSi10Mg and Scalmalloy, in different heat-treated (HT) conditions i.e., stress-relief, T6, and hot isostatic pressing (HIP), as well as the non-heat-treated condition. The microstructures were examined using scanning electron microscope, and the mechanical properties were evaluated using uniaxial tensile testing. For AlSi10Mg, Si-networks were observed to break down, and Si- and Fe-rich particles precipitates form during HIP followed by T6. For Scalmalloy, the density of nanometer-sized intergranular $Al_3(Sc_xZr_{1-x})$ precipitates increased after only HIP. Furthermore, it was observed that the addition of HIP improved the tensile strengths of both alloys as compared to their AM as well as wrought counterparts in similar HT conditions.

Keywords: Laser powder bed fusion (L-PBF), AlSi10Mg, Scalmalloy, Hot isostatic pressing (HIP), Microstructure, Tensile properties

Introduction

Additive manufacturing (AM) allows the fabrication of complex shapes by layer-by-layer process [1]. The laser powder bed fusion (L-PBF) is a widely used AM technology for various Al alloys such as AlSi10Mg. Al alloys are well known in different industries, including automotive, aerospace, construction, and packaging, due to their superior material properties such as light-weight, good corrosion resistance, high thermal conductivity, excellent machinability, etc. [2–4]. AM of Al alloys could be more challenging than other metals because Al powder particles are naturally light and have high moisture absorption, high thermal conductivity, and high oxidation

tendency, all of which may affect the fabrication process and therefore, resulting in detrimental process-induced defects on the mechanical properties of the AM Al components [5].

AlSi10Mg is one of the most popular and widely used Al alloys in AM industry. Characterized by low coefficient of thermal expansion (CTE), AlSi10Mg components can be manufactured by AM with great dimensional precision and low thermal stresses. Post-processing heat treatments (HT) are frequently used for AM metals to partly alleviate the detrimental effect of some characteristics. These include the dendritic microstructure that improves the mechanical properties of alloys [6].

There are several research in the literature studying the effect of different thermal post-processes on microstructure and mechanical properties of L-PBF AlSi10Mg [7–13]. The conventional HT for the AM AlSi10Mg alloy consists of two steps: (1) T4: solid solution (at 540°C for 6 hr, then water quench) followed by (2) T6: artificial ageing (at 160°C for 4 hr, then air cool) [7–9]. The T4 HT could have complete homogenization effect on microstructure while T6 could improve the strength of the L-PBF AlSi10Mg alloy. Nonetheless, EOS merely recommends a low temperature stress relieving (SR) at 300°C for 2 hr [12]. It should be noted that the hot isostatic pressing (HIP), as common HT for certain AM metals, could also be used for L-PBF AlSi10Mg. But having HIP along may cause a significant strength reduction with remarkably increased ductility for L-PBF AlSi10Mg [13].

Scalmalloy is a Sc- and Zr- modified high strength Al alloy, which has received a lot of attention by AM industries [14–18]. The L-PBF Scalmalloy have shown a bimodal grain structure consisting of nano-size equiaxed grains as well as fine columnar grains [15]. The conventional annealing HT for Scalmalloy is a low temperature HT at 325°C for 4 hr. [17, 18], resulting in nanometer-sized Al_3(Sc, Zr) precipitation along the grain boundaries which prevents grain growth [16].

HIP is widely recognized for its ability to reduce volumetric defects in the material or even removing them. HIP alone or followed by appropriate HT schedule could modify the tensile properties and which in turn, improves the fatigue resistance of the materials. In this article, the effect of HIP treatment for both L-PBF AlSi10Mg and L-PBF Scalmalloy were investigated and compared with the typical conventional HT on microstructure and tensile properties of the alloys.

Experimental Procedure

Material and Fabrication

Cylindrical bars (15 mm in diameter by 90 mm in height) of AlSi10Mg and Scalmalloy were fabricated using L-PBF techniques, by Valimet [19] and Heraus Additive Manufacturing [20], respectively. The chemical compositions of AlSi10Mg and Scalmalloy powders are presented in **Table 1**. Furthermore, **Table 2** presents the process parameters used in this study for the fabrication of cylindrical bars, provided by the manufacturer. Small coupons (5 mm thickness) were cut from cylindrical bars for further microstructural analysis.

Table 1. Chemical composition of AlSi10Mg powder, provided by Valimet [19] and Scalmalloy powder, provided by Heraeus Additive Manufacturing [20].

		Si	Mg	Fe	Cu	Mn	Ti	Zn	Ni	Others	Al
AlSi10Mg	wt. %	10.2	0.3	0.09	0.002	0.002	0.011	0.004	0.006	< 0.10	Bal

		Mg	Sc	Zr	Mn	Si	Fe	Zn	Cu	Ti	V
Scalmalloy	wt. %	4.29	0.7	0.32	0.59	0.053	0.099	0.004	0.002	0.018	0.01
		O	**Al**								
	wt. %	0.05	Bal								

Table 2. Process parameters used for fabricating the L-PBF AlSi10Mg and L-PBF Scalmalloy.

Material	Laser power (W)	Scan speed (mm/s)	Hatch distance (µm)	Layer thickness (µm)
AlSi10Mg	370	1480	120	60
Scalmalloy	380	1425	145	30

The multi-steps heat treatment schedules used in this study for the both alloys are listed in **Table 3**, which are also schematically shown in **Figure 1**. Following the ASTM F3301-18a [21] and AMS 2771F [22] standards, the heat treatment schedules were selected. The heat treatment was performed under an argon-atmosphere in an electric furnace.

Table 3. Different post-process HTs used in this study.

Material	HT	SR	HIP	T6 (Solution + Aging)
AlSi10Mg	SR+HIP+T6	270°C/1.5 hr/FC	520°C/100 MPa/2 hr/FC	540°C/6 hr./WQ + 160°C/4 hr/AC
	SR+T6	270°C/1.5 hr/FC	---	540°C/6 hr./WQ + 160°C/4 hr/AC
Scalmalloy	SR	325°C/4 hr/FC	---	---
	HIP	---	325°C/100 MPa/4 hr/FC	---

Notes: FC: Furnace Cool, WQ: Water Quench, AC: Air Cool

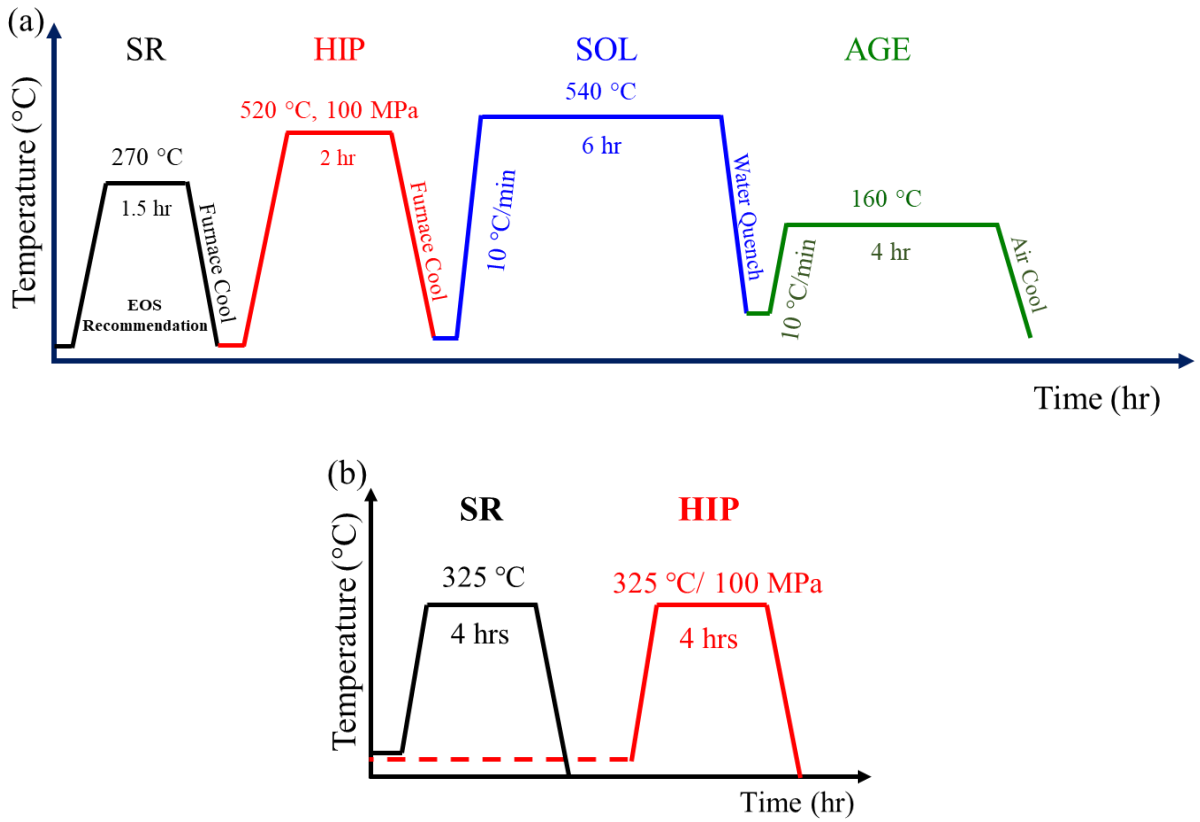

Figure 1. Schematic diagrams of HT schedules conducted on (a) L-PBF AlSi10Mg and (b) L-PBF Scalmalloy.

Microstructure characterization

Microstructural characterization was conducted in the transverse direction (TD) plane, i.e., parallel to the build direction. The metallography procedures were performed according to the ASTM-E3 [23] including cold-mounting, grinding with SiC sandpapers with grits sizes ranging from 320 to 4000, and polishing to a mirror-finished surface using polishing cloths and colloidal silica suspensions size of 0.05 µm. Electron backscatter diffraction (EBSD) analysis and electron channeling contrast imaging (ECCI) were conducted for microstructure characterization using a Zeiss Cross Beam 550 scanning electron microscope (SEM).

Mechanical testing

The cylindrical bars were machined upon HTs to the final geometry of uniaxial tensile tests (see **Figure 2**) according to the ASTM E8 [24]. The room temperature tensile tests were performed using an MTS landmark servo-hydraulic load frame with a load cell of 100 kN. The quasi-static tensile tests were conducted in two steps: strain-controlled followed by displacement-controlled step. An MTS mechanical extensometer was attached to the specimen in the gage section to record the strain. However, due to the limited travel range of the extensometer, it was removed at ~0.035 mm/mm strain by pausing the test, after which the test was resumed in the displacement-controlled

mode up to fracture. At least three tests for each HT condition were conducted to ensure the repeatability of the results.

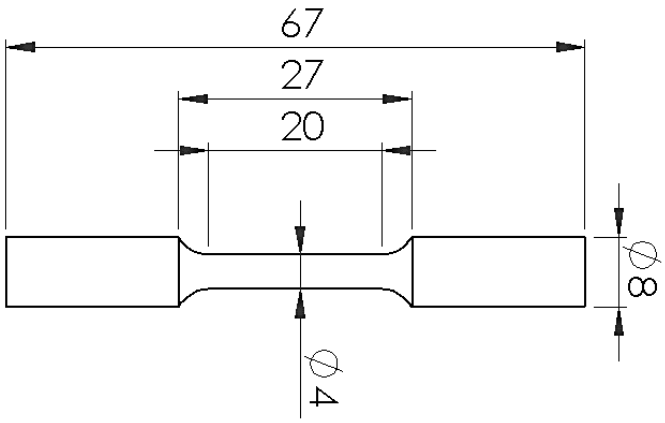

Figure 2. The geometry of the tensile specimens following ASTM E8 [24]

Results and Discussion

Microstructure analysis

The Inverse Pole Figure (IPF) maps for the non-heat treated (NHT) and HT of the both L-PBF AlSi10Mg and Scalmalloy obtained from EBSD analysis are presented in **Figure 3** (a) to (c) and (d) to (f), respectively. The IPF maps were obtained in the transverse direction (TD) plane (i.e., parallel to the build direction. On one hand, for L-PBF AlSi10Mg, the grain structure was mostly columnar which is typical for AM metal alloys [25]. As shown in **Figure 3(a)-(c)**, the average grain sizes were affected by the HTs, i.e., ~ 2.9 μm for the NHT condition, ~ 5.3 μm for SR+T6, and for ~ 10.6 μm SR+HIP+T6.

On the other hand, the L-PBF Scalmalloy showed much finer grain structure with bi-modal morphology consisting of (1) nano-sized equiaxed fine grains (FG) along melt pool boundaries and (2) coarser grain (CG) away from melt pool (see **Figure 3(d)-(f)**). The average grain sizes of the L-PBF Scalmalloy in different HT conditions did not show significant changes, ranging from 3.8, 2.8 and 5.6 μm for NHT, SR, and HIP conditions, respectively. The presence of such fine grain structure in NHT condition could be attributed to the rapid solidification rate during the L-PBF process [26]. Upon HTs, similar fine grain structure is maintained which is attributed to the precipitation of nano-size Al_3Sc and Al_3Zr particles, which can act as grain growth inhibitors [27]. It is worth noting that the actual value of the average grain sizes for the L-PBF Scalmalloy may be significantly smaller than what was reported using EBSD analysis due to step size limit (0.43 μm).

The BSE micrographs obtained by ECCI technique for both the alloys are presented in **Figure 4** in all the different HT conditions investigated in this study. As shown in **Figure 4(a)**, NHT condition of L-PBF AlSi10Mg consisted of the cellular Si network. Upon HTs, these networks break down and form bulky Si-rich and needle shaped Fe-rich particles at grain boundaries (GB) and grain interiors (see **Figure 4(b)-(d)**) [7,28]. Furthermore, due homogenization of high temperature solutionizing (T4) or HIP stages, the micro-segregation of Si and Mg elements that were observed in the NHT specimens (see **Figure 4(a)**) are completely dissolved back into the α-Al matrix, resulting in supersaturated solid solution (SSSS). It should be

noted that during the subsequent age hardening T6 step, the nanometer-sized Mg_2Si particles could precipitate from the SSSS matrix, which are only detectable by transmission electron microscopy (TEM) therefore are not shown over here [29].

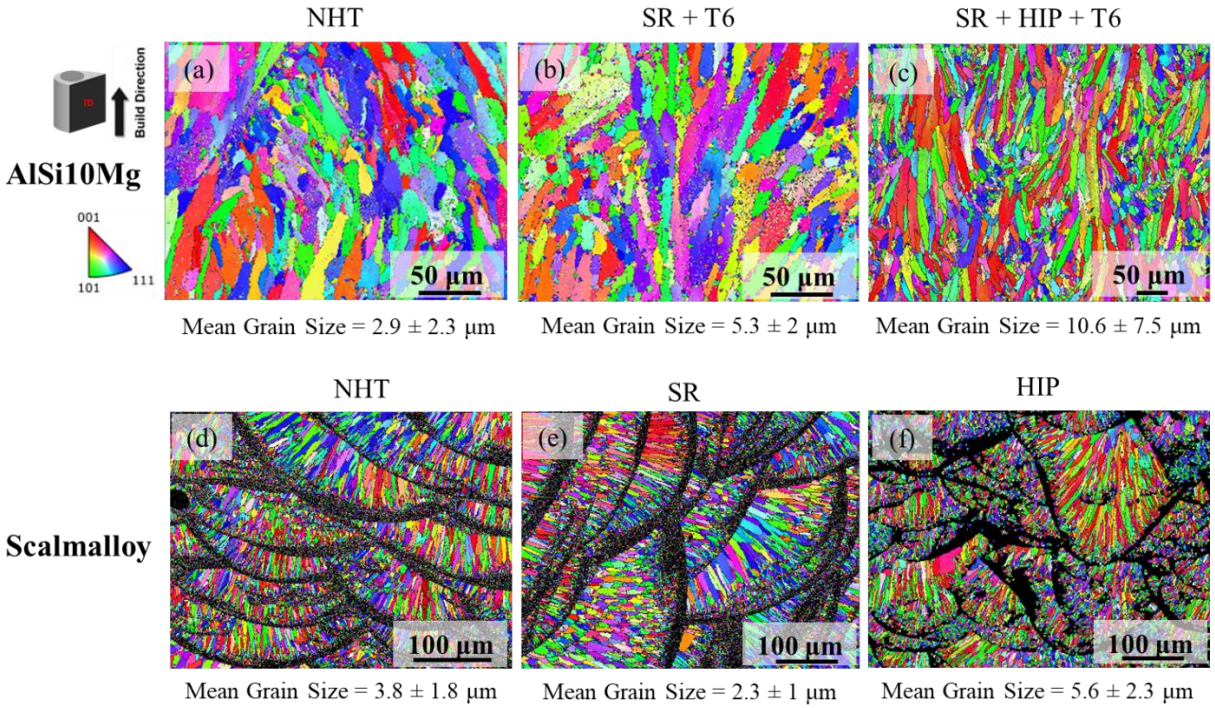

Figure 3. Inverse pole figure (IPF) maps obtained by EBSD analysis in the TD plane in (a) to (c) for the L-PBF AlSi10Mg and in (d) to (f) for the L-PBF Scalmalloy in different heat treatment conditions investigated in this study.

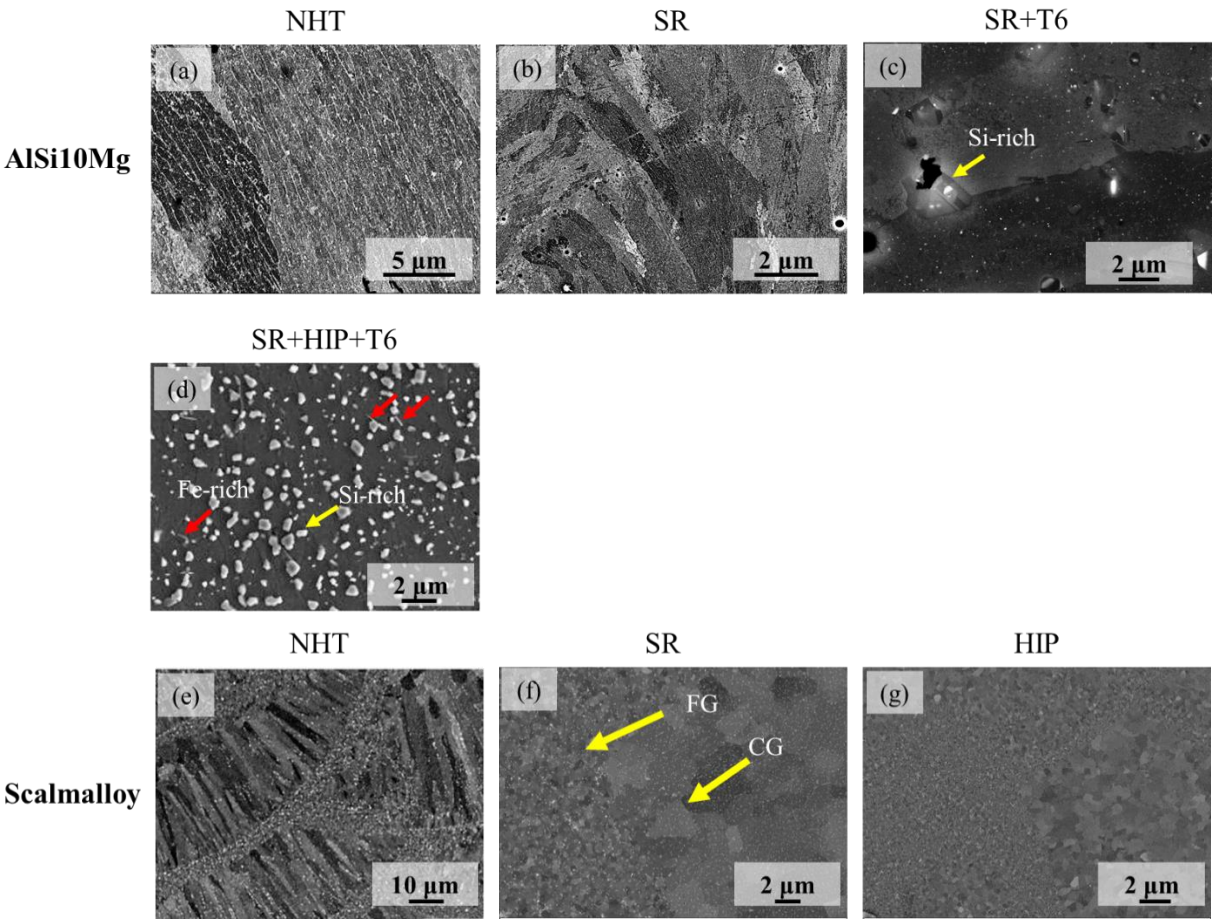

Figure 4. BSE micrographs obtained in TD for (a)-(d) L-PBF AlSi10Mg and (e)-(g) L-PBF Scalmalloy in different heat treatment conditions.

For L-PBF Scalmalloy, upon SR and HIP, the fine inter dendritic regions are partially dissolved back into the α-Al matrix (see **Figure 4(e)-(f)**). However, as discussed earlier, the formation of small $Al_3(Sc, Zr)$ phases at GBs during the low temperature SR and HIP as GB boundary strengthening particles help the alloy maintain the prior fine grain structure observed in NHT condition.

Tensile properties

The uniaxial tensile properties including yield strength (YS), ultimate tensile strength (UTS) and percent elongation to failure (%EL) are presented as a column chart in **Figure 5** (a) and (b) for L-PBF AlSi10Mg alloy and L-PBF Scalmalloy, respectively. In addition, the tensile properties of cast AlSi10Mg [30] and wrought Scalmalloy [31] are also included for comparison purposes.

It can be seen in **Figure 5** (a) that tensile strengths (e.g., YS and UTS) and %EL of L-PBF AlSi10Mg in SR condition was significantly higher than those of cast counterpart by ~87%, 44% and 170%, respectively, which could be attributed to the typical columnar fine grain structure observed for the former (see **Figure 4(b)**) [32-33]. As discussed earlier, upon T6, due to formation

of Si-rich and Fe-rich particles precipitate at GBs and grain interiors as well as small Mg_2Si precipitates [7, 28], the tensile YS of the alloy is increased by ~12% which is compromised with a decrease in EL [10, 34]. Moreover, as it can be seen the intermediate HIP prior to T6 heat treatment showed relatively small impacts on tensile strengths of the alloy while it resulted in significant improvement on %EL of the alloy which could be attributed to the effect of HIP on closing the process induced pores [13,35].

It can also be observed that tensile strength of L-PBF Scalmalloy in SR condition is significantly higher as compared to the wrought counterpart (see **Figure 5(b)**). The YS and UTS are increased by ~60% and ~31%, respectively, which could be attributed to the nano-sized grain structure as well as Al_3(Sc, Zr) precipitates [33,36]. However, the EL was compromised and significantly decreased from 20% to 1.4%. Upon further HT, the tensile properties were affected insignificantly.

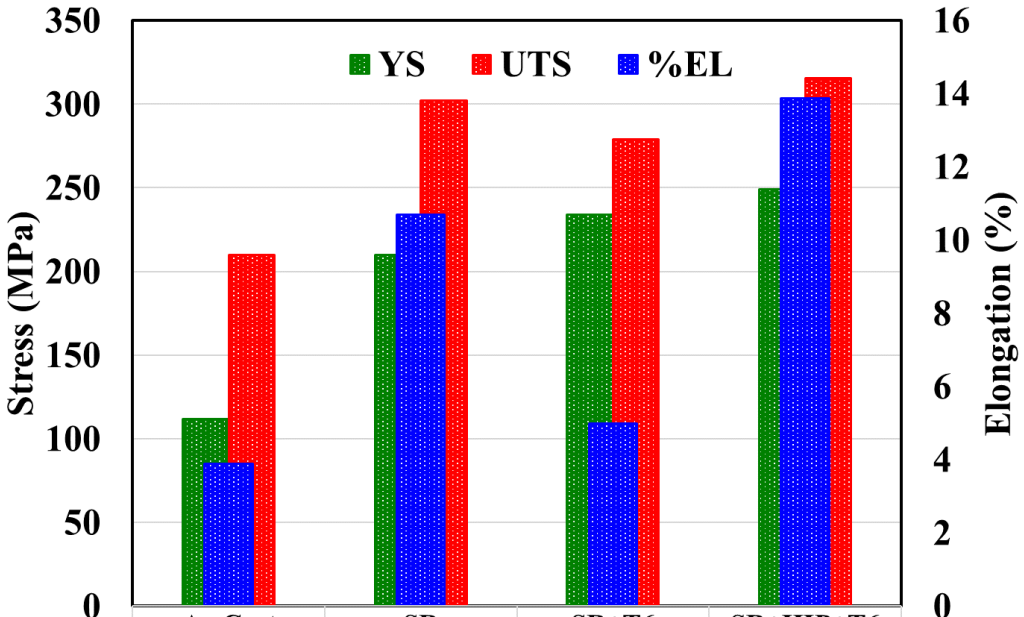

	As-Cast	SR	SR+T6	SR+HIP+T6
YS	112	210	234	249.08
UTS	210	302	279	315.62
%EL	3.9	10.7	5	13.88

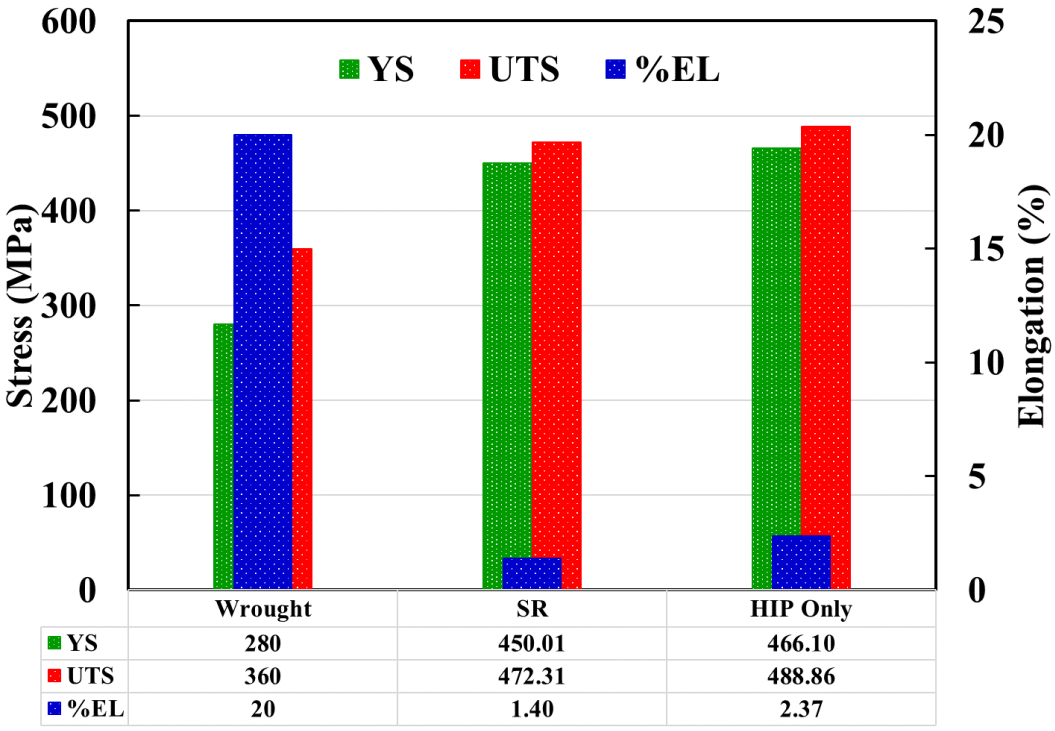

	Wrought	SR	HIP Only
YS	280	450.01	466.10
UTS	360	472.31	488.86
%EL	20	1.40	2.37

Figure 5. Bar chart representation of the tensile properties of (a) AlSi10Mg and (b) Scalmalloy under different heat treatment conditions investigated in this study.

Conclusions

In this study, the effect of different heat treatments on microstructure and tensile properties of AlSi10Mg and Scalmalloy fabricated by L-PBF are investigated. The test specimens underwent different post thermal processing including stress-relief (SR), followed by hot isostatic pressing (HIP) and T6 for L-PBF AlSi10Mg. For L-PBF Scalmalloy, the heat treatments were SR and HIP. The microstructure was characterized between each two steps of the multi-step heat treatments. Furthermore, the tensile properties were evaluated through the quasi-static tensile testing. The experimental observations from this study can be concluded as follows:

1. Grain growth was seen for both L-PBF AlSi10Mg after the different post process heat treatment. For L-PBF AlSi10Mg, the grains are typically columnar and after SR+HIP+T6, the grain size increased even further than the SR+T6 condition. A bi-modal grain structure is observed consisting of nano-sized equiaxed grains along the melt pool boundaries for L-PBF Scalmalloy, which become more finer with partially elongated grains after HIP process.
2. A cellular network of Si phase was seen for non-heat-treated (NHT) L-PBF AlSi10Mg. The Si-networks dissolved after SR+T6 heat treatment and even after SR+HIP+T6, Si-particles and Fe-rich particles precipitates. For L-PBF Scalmalloy, the Sc and Zr elements

are accumulated and distributed in the matrix after SR, and even after HIP process the strong Al_3(Sc, Zr) phase precipitates.

3. The tensile strength and ductility increased after SR+HIP+T6 for L-PBF AlSi10Mg compared to SR+T6 condition because of fine Si- and Fe-rich particles precipitates. The L-PBF Scalmalloy showed higher strength and ductility after HIP.

Acknowledgment

This research is partially supported by the National Aeronautics and Space Administration NASA under Cooperative Agreement No. 80MSFC19C0010. This paper describes objective technical results and analysis. Any subjective views or opinions that might be expressed in the paper do not necessarily represent the views of the National Aeronautics and Space Administration (NASA) or the United States Government.

References

[1] Gibson I, Rosen D, Stucker B, Khorasani M. Additive Manufacturing Technologies. 3rd ed. New York: Springer, Cham; 2021.

[2] Martin JH, Yahata BD, Hundley JM, Mayer JA, Schaedler TA, Pollock TM. 3D printing of high-strength aluminium alloys. Nature 2017;549:365–9. https://doi.org/10.1038/nature23894.

[3] Rendigs KH. Aluminium Structures Used in Aerospace - Status and Prospects-. Alum. Alloy. - Suppl. ICAA5, vol. 242, Trans Tech Publications Ltd; 1997, p. 11–24. https://doi.org/10.4028/www.scientific.net/MSF.242.11.

[4] Zhang J, Song B, Wei Q, Bourell D, Shi Y. A review of selective laser melting of aluminum alloys: Processing, microstructure, property and developing trends. J Mater Sci Technol 2019;35:270–84. https://doi.org/https://doi.org/10.1016/j.jmst.2018.09.004.

[5] Louvis E, Fox P, Sutcliffe CJ. Selective laser melting of aluminium components. J Mater Process Technol 2011;211:275–84. https://doi.org/https://doi.org/10.1016/j.jmatprotec.2010.09.019.

[6] Bagherifard S, Beretta N, Monti S, Riccio M, Bandini M, Guagliano M. On the fatigue strength enhancement of additive manufactured AlSi10Mg parts by mechanical and thermal post-processing. Mater Des 2018;145:28–41. https://doi.org/https://doi.org/10.1016/j.matdes.2018.02.055.

[7] Aboulkhair NT, Maskery I, Tuck C, Ashcroft I, Everitt NM. The microstructure and mechanical properties of selectively laser melted AlSi10Mg: The effect of a conventional T6-like heat treatment. Mater Sci Eng A 2016;667:139–46. https://doi.org/https://doi.org/10.1016/j.msea.2016.04.092.

[8] Maskery I, Aboulkhair NT, Tuck C, Wildman RD, Ashcroft IA, Everitt NM, et al. Fatigue performance enhancement of selectively laser melted aluminium alloy by heat treatment. Proc - 26th Annu Int Solid Free Fabr Symp - An Addit Manuf Conf SFF 2015 2020:1017–

25.

[9] Wang LF, Sun J, Yu XL, Shi Y, Zhu XG, Cheng LY, et al. Enhancement in mechanical properties of selectively laser-melted AlSi10Mg aluminum alloys by T6-like heat treatment. Mater Sci Eng A 2018;734:299–310. https://doi.org/https://doi.org/10.1016/j.msea.2018.07.103.

[10] Tang M, Pistorius PC. Oxides, porosity and fatigue performance of AlSi10Mg parts produced by selective laser melting. Int J Fatigue 2017;94:192–201. https://doi.org/https://doi.org/10.1016/j.ijfatigue.2016.06.002.

[11] Pierre VC, Gokula KM, Pierrick B, Lore T, Brecht VH, Kim V. Reducing hydrogen pores and blisters by novel strategies and tailored heat treatments for laser powder bed fusion of AlSi7Mg0.6. Euro PM 2019 Congr Exhib 2019:1–7.

[12] EOS. EOS Aluminium AlSi10Mg Material Data Sheet 2014;49:1–5.

[13] Hirata T, Kimura T, Nakamoto T. Effects of hot isostatic pressing and internal porosity on the performance of selective laser melted AlSi10Mg alloys. Mater Sci Eng A 2020;772:138713. https://doi.org/https://doi.org/10.1016/j.msea.2019.138713.

[14] APWORKS AIRBUS GmbH. Scalmalloy-state of the art high-strength alloy 2017.

[15] Zhou L, Pan H, Hyer H, Park S, Bai Y, McWilliams B, et al. Microstructure and tensile property of a novel AlZnMgScZr alloy additively manufactured by gas atomization and laser powder bed fusion. Scr Mater 2019;158:24–8. https://doi.org/https://doi.org/10.1016/j.scriptamat.2018.08.025.

[16] Spierings AB, Dawson K, Kern K, Palm F, Wegener K. SLM-processed Sc- and Zr-modified Al-Mg alloy: Mechanical properties and microstructural effects of heat treatment. Mater Sci Eng A 2017;701:264–73. https://doi.org/https://doi.org/10.1016/j.msea.2017.06.089.

[17] Begoc S, Montredon F, Pommatau G, Leger G, Gas M, Eyrignoux S. Additive manufacturing of Scalmalloy® satellite parts. Proc 8th Eur Conf Aeronaut Sp Sci 2019:1–15. https://doi.org/10.13009/EUCASS2019-677.

[18] Baig S, Ghiaasiaan SR, Shamsaei N. Effect of Heat Treatment on the Microstructure and Mechanical Properties of LB-PBF AlSi10Mg and Scalmalloy. In: Perander L, editor. Light Met. 2021, Cham: Springer International Publishing; 2021, p. 119–25.

[19] Spherical Aluminum Powders | Valimet n.d. https://valimet.com/spherical-aluminum-powders/ (accessed May 27, 2022).

[20] 3D Printing with metals n.d. https://www.heraeus.com/en/hpm/hmp_products_solutions/3_d_printing/additive_manufacturing_home/home_additive_manufacturing.html (accessed May 27, 2022).

[21] ASTM F3301-18a. Standard for Additive Manufacturing – Post Processing Methods – Standard Specification for Thermal Post-Processing Metal Parts Made Via Powder Bed Fusion. ASTM Stand 2018:3. https://doi.org/10.1520/F3301-18A.2.

[22] SAE International. AMS2771F: Heat Treatment of Aluminum Alloy Castings 2017. https://www.sae.org/standards/content/ams2771f/ (accessed May 27, 2022).

[23] Interanational AE− 11 (Reapproved 2017). Standard Guide for Preparation of Metallographic Specimens Standard Guide for Preparation of Metallographic Specimens 1. ASTM Int 2012;03.01:1–12. https://doi.org/10.1520/E0003-11R17.1.

[24] ASTM International. ASTM E8/E8M standard test methods for tension testing of metallic materials. West Conshohocken, PA 19428-2959 USA 2013. https://doi.org/10.1520/E0008.

[25] Li X, Yi D, Wu X, Zhang J, Yang X, Zhao Z, et al. Effect of construction angles on microstructure and mechanical properties of AlSi10Mg alloy fabricated by selective laser melting. J Alloys Compd 2021;881:160459. https://doi.org/https://doi.org/10.1016/j.jallcom.2021.160459.

[26] Isaac JP, Lee S, Shamsaei N, Tippur H V. Dynamic fracture behavior of additively manufactured Scalmalloy®: Effects of build orientation, heat-treatment and loading-rate. Mater Sci Eng A 2021;826:141978. https://doi.org/https://doi.org/10.1016/j.msea.2021.141978.

[27] Kuo CN, Peng PC, Liu DH, Chao CY. Microstructure Evolution and Mechanical Property Response of 3D-Printed Scalmalloy with Different Heat-Treatment Times at 325 °C. Metals (Basel) 2021;11. https://doi.org/10.3390/met11040555.

[28] Özer G, Tarakçi G, Yilmaz MS, Öter ZÇ, Sürmen Ö, Akça Y, et al. Investigation of the effects of different heat treatment parameters on the corrosion and mechanical properties of the AlSi10Mg alloy produced with direct metal laser sintering. Mater Corros 2020;71:365–73. https://doi.org/https://doi.org/10.1002/maco.201911171.

[29] Hadadzadeh A, Amirkhiz BS, Mohammadi M. Contribution of Mg2Si precipitates to the strength of direct metal laser sintered AlSi10Mg. Mater Sci Eng A 2019;739:295–300. https://doi.org/https://doi.org/10.1016/j.msea.2018.10.055.

[30] Yan Q, Song B, Shi Y. Comparative study of performance comparison of AlSi10Mg alloy prepared by selective laser melting and casting. J Mater Sci Technol 2020;41:199–208. https://doi.org/https://doi.org/10.1016/j.jmst.2019.08.049.

[31] Filatov Y., Yelagin VI, Zakharov V V. New Al–Mg–Sc alloys. Mater Sci Eng A 2000;280:97–101. https://doi.org/https://doi.org/10.1016/S0921-5093(99)00673-5.

[32] Shakil SI, Hadadzadeh A, Shalchi Amirkhiz B, Pirgazi H, Mohammadi M, Haghshenas M. Additive manufactured versus cast AlSi10Mg alloy: Microstructure and micromechanics. Results Mater 2021;10:100178. https://doi.org/https://doi.org/10.1016/j.rinma.2021.100178.

[33] Muhammad M, Nezhadfar PD, Thompson S, Saharan A, Phan N, Shamsaei N. A comparative investigation on the microstructure and mechanical properties of additively manufactured aluminum alloys. Int J Fatigue 2021;146:106165. https://doi.org/https://doi.org/10.1016/j.ijfatigue.2021.106165.

[34] Nezhadfar PD, Thompson S, Saharan A, Phan N, Shamsaei N. Structural integrity of additively manufactured aluminum alloys: Effects of build orientation on microstructure,

porosity, and fatigue behavior. Addit Manuf 2021;47:102292. https://doi.org/https://doi.org/10.1016/j.addma.2021.102292.

[35] Ertuğrul O, Öter ZÇ, Yılmaz MS, Şahin E, Coşkun M, Tarakçı G, et al. Effect of HIP process and subsequent heat treatment on microstructure and mechanical properties of direct metal laser sintered AlSi10Mg alloy. Rapid Prototyp J 2020;26:1421–34. https://doi.org/10.1108/RPJ-07-2019-0180.

[36] Koutny D, Skulina D, Pantělejev L, Paloušek D, Lenczowski B, Palm F, et al. Processing of Al-Sc aluminum alloy using SLM technology. Procedia CIRP 2018;74:44–8. https://doi.org/https://doi.org/10.1016/j.procir.2018.08.027.